

Multicolour observations of V404 Cyg with ULTRACAM

T. Shahbaz,^{1*} V.S. Dhillon², T.R. Marsh³, C. Zurita¹, C. A. Haswell⁴, P.A. Charles³
R.I. Hynes⁵, J. Casares¹

¹*Instituto de Astrofísica de Canarias, 38200 La Laguna, Tenerife, Spain*

²*Department of Physics and Astronomy, University of Sheffield, Sheffield, S3 7RH, UK*

³*Department of Physics and Astronomy, University of Southampton, Southampton, SO17 1BJ, UK*

⁴*Department of Physics and Astronomy, The Open University, Walton Hall, Milton Keynes, MK7 6AA*

⁵*Astronomy Department, The University of Texas at Austin, 1 University Station C1400, Austin, Texas 78712-0259, USA*

29 October 2018

ABSTRACT

We present high time-resolution multicolour observations of the quiescent soft X-ray transient V404 Cyg obtained with ULTRACAM. Superimposed on the secondary star’s ellipsoidal modulation are large flares on timescales of a few hours, as well as several distinct rapid flares on timescales of tens of mins. The rapid flares, most of which show further variability and unresolved peaks, cover shorter timescales than those reported in previous observations. The power density spectrum (PDS) of the 5 s time-resolution data shows a quasi-periodic oscillation (QPO) feature at 0.78 mHz (=21.5 min). Assuming this periodicity represents the Keplerian period at the transition between the thin and advective disc regions, we determine the transition radius. We discuss the possible origins for the QPO feature in the context of the advection-dominated accretion flow model.

We determine the colour of the large flares and find that the i' band flux per unit frequency interval is larger than that in the g' band. The colour is consistent with optically thin gas with a temperature of ~ 8000 K arising from a region with an equivalent blackbody radius of at least $2 R_{\odot}$, which covers 3 percent of the accretion disc’s surface. Our timing and spectral analysis results support the idea that the rapid flares (i.e. the QPO feature) most likely arise from regions near the transition radius.

Key words: accretion, accretion discs – binaries: close – stars: individual: V404 Cyg

1 INTRODUCTION

Soft X-ray transients (SXTs) are a subclass of low-mass X-ray binaries (LMXBs) that are characterized by episodic, dramatic X-ray and optical outbursts, which usually last for several months and recur on a timescale of decades. In the interim the SXTs are in a state of quiescence during which the optical emission is dominated by the luminosity of the faint companion star (van Paradijs & McClintock 1995). In quiescence the optical lightcurves exhibit the classical double-humped ellipsoidal modulation, which is due to the differing aspects that the tidally distorted secondary star presents to the observer throughout its orbit (Shahbaz et al. 2003).

In outburst the high/soft and the low/hard X-ray states are commonly seen. In the high/soft state, X-ray emission is dominated by thermal emission from an accretion disc extending close to the last stable orbit around a black hole. In the low/hard state, the inner disc is believed to be truncated

and emission appears to arise from an extended corona. Similar ideas are involved for the advective models proposed for the quiescent state (Narayan, Garcia & McClintock 2001), but with the disc truncated at larger radii. The states of SXTs are also classified by their X-ray timing properties; the high/soft state shows low level red noise, whereas the low/hard state and very high states exhibit band-limited noise but with a low-frequency break at ~ 0.02 –30 Hz, and sometimes superposed QPOs (see van der Klis 1995 and Wijnands & van der Klis 1999).

Although the spectral and timing properties during the quiescent state have not been well studied, one might expect similar properties, as the structure of the flow is believed to be similar to that in the low/hard state. The relatively high quiescent X-ray luminosity of V404 Cyg with respect to other SXTs indicates that there is still some continuing accretion. This is also supported by the short-term variability seen at all wavelengths in several quiescent photometric studies of V404 Cyg (Pavlenko et al. 1996; Zurita, Casares & Shahbaz 2003). Sub-orbital variability with an amplitude

* E-mail: tsh@ll.iac.es

Table 1. Log of ULTRACAM observations.

Date	Run #	# pts	Exposure Time (s)	JD 2452520.5 + start – end	Orbital phase mid	g'	i'	Comments
09/9/02	run 09(a)	1200	5.0	26.96793 – 27.05119	0.855	19.836	16.570	Poor seeing at end of night
10/9/02	run 10(a)	1266	5.0	27.87320 – 27.94646	0.993	19.755	16.615	
10/9/02	run 10(b)	1152	5.0	27.97038 – 28.03704	0.159	19.920	16.658	Good seeing
12/9/02	run 12(a)	1192	5.0	29.85483 – 29.92379	0.293	19.545	16.406	
12/9/02	run 12(b)	1282	5.0	29.92406 – 29.99824	0.310	19.641	16.467	
12/9/02	run 12(c)	848	5.0	29.99853 – 30.04770	0.316	19.695	16.516	
13/9/02	run 13(a)	1082	5.0	30.83847 – 30.90107	0.451	19.968	16.690	
13/9/02	run 13(b)	948	5.0	30.90135 – 30.92339	0.460	19.879	16.656	
14/9/02	run 14(a)	8544	0.237	31.83812 – 31.86152	0.602	-	16.768	
14/9/02	run 14(b)	2791	0.237	31.86162 – 31.86902	0.605	-	16.669	Noisy data, not used in PDS
14/9/02	run 14(c)	9155	0.237	31.86936 – 31.89443	0.607	-	16.649	”
14/9/02	run 14(d)	7236	0.237	31.89942 – 31.91924	0.611	-	16.754	
14/9/02	run 14(e)	8773	0.237	31.91932 – 31.94334	0.615	-	16.708	

of 0.10–0.20 mag (Wagner et al. 1994) which is partly due to a ~ 6 hr quasi-periodic oscillation (Casares et al. 1993; Pavlenko et al. 1996) is present in the optical. The $H\alpha$ line profile also changes significantly on short timescales (Casares & Charles 1992) and seems to be correlated with the continuum (Hynes et al. 2002). Short timescale variations also appear in the infrared (Sanwal et al. 1996). At X-ray energies, *ROSAT* (0.1–2.4 keV) saw changes of a factor of 10 on timescales < 0.5 day. More recent observations with *Chandra* (0.3–7 keV) showed variability of a factor of 2 in a few msec (Kong et al. 2002). Finally V404 Cyg is also a variable radio source on timescales of days, with typical variability in flux of 0.1–0.8 mJy (Hjellming 2000).

The origin of the variability remains uncertain, the most likely explanations are magnetic reconnection events in the disc or optical emission from an advective region. The other possibilities such as reprocessed X-ray variability and flickering from the accretion stream impact point are less likely (Zurita et al. 2003). To determine if just one type of variability dominates or if the variability is a combination of mechanisms on different timescales, it is therefore important to perform a comparative study of the class.

In the optical, the faintness of the SXTs has usually limited the time resolution one can practically achieve. Furthermore, observations have normally been constrained to a single waveband. ULTRACAM with 4-m class telescopes provides a unique opportunity not only to study photometric variability on the shortest timescales, but also in more than one waveband simultaneously. Therefore we have embarked upon a programme to study the fast multicolour variability of quiescent SXTs with ULTRACAM. Our main aims are to study the multicolour variability of the brighter SXTs and to study variability in the fainter ones, faster than previously possible. We present here high time resolution multicolour observations of one of the brightest SXTs, V404 Cyg.

2 OBSERVATIONS AND DATA REDUCTION

Multicolour photometric observations of V404 Cyg were taken with ULTRACAM on the William Herschel Telescope

atop La Palma during the period 2002 Sep 9 to 13. ULTRACAM is an ultra-fast, triple-beam CCD camera. The light is split into three wavelengths colours (blue, green and red) by two dichroic beamsplitters and then passes through a filter. The detectors are three back-illuminated, thinned, Marconi frame-transfer 1024×1024 active area CCD chips with a pixel scale of 0.3 arcsecs/pixel. The CCDs are cooled using a three-stage peltier device and water chiller, resulting in negligible dark current (especially at these short integration times). With the frame transfer mode, the dead-time is essentially zero (for further details see Dhillon & Marsh 2001).

Our observations were taken using the Sloan u' , g' and i' filters with effective wavelengths of 3550 Å, 4750 Å and 7650 Å respectively. For the first 5 nights (Sep 9 to 12), we used an exposure time of 5.0 sec, which was short enough to give reasonable counts in the g' and i' bands. Given the faintness of the object ($B=20.6$, $V=18.4$) and the short exposure times, few counts were obtained in the u' band. On the last night (Sep 13) we decreased the exposure time to 0.237 sec. Only data in the i' band were usable. From hereafter, we will refer to the data taken with exposure times of 5.0 sec and 0.237 sec as the “slow” and “fast” data respectively.

The weather conditions during the observing run were on the whole very good. The night of Sep 9 suffered from severe seeing ($2''$) during the end of the night. No useful data could be obtained on Sep 11 due to cloud. The night of Sep 10 was photometric, so we observed the flux standard BD+35 3659 (Smith et al. 2002) in order to determine the u' , g' and i' band instrumental zeropoints, which were then used to calibrate the data. On Sep 14, due to an earthing problem, the electronic bias level occasionally increased by a factor of 2, however, this only affected runs 14(b) and (c). A log of the observations is given in Table 1.

The pipeline reduction procedures were used to debias and flat-field the data. The same pipeline was also used to determine lightcurves for V404 Cyg and several comparison stars by extracting the counts using aperture photometry. As there is a line-of-sight contaminating star 1.5 arcsec North of V404 Cyg, we obtained the combined counts using an aperture sufficient enough to encompass both stars. We

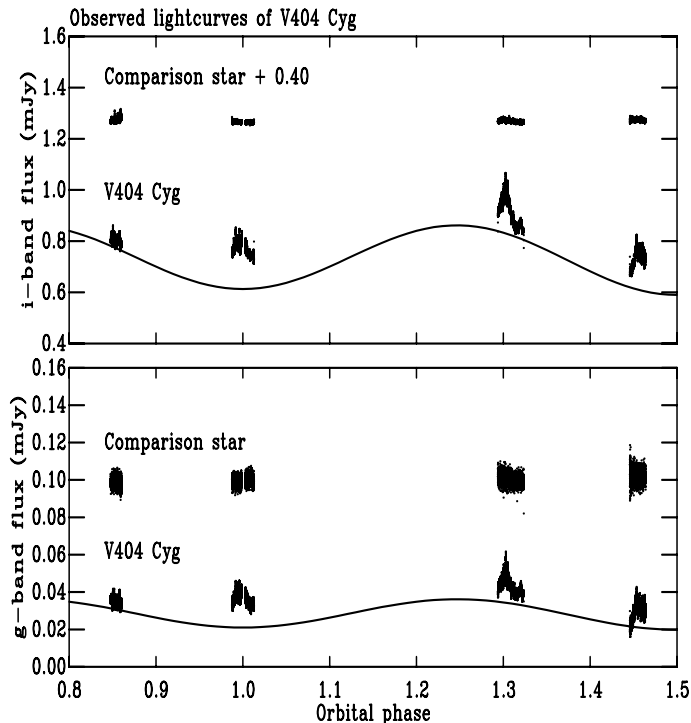


Figure 1. The observed g' and i' flux lightcurves of V404 Cyg and the comparison star. The solid line is the secondary star's ellipsoidal modulation (see text).

determined lightcurves with different sized apertures, ranging from 1.8 to 4.2 arcsec. The optimal and most reliable results, given the contaminating star, were obtained using a large aperture of 3 arcsec. The count ratio of V404 Cyg with respect to the local standard (3.6" S 75.8" E of V404 Cyg) was then determined by subtracting the count ratio of the contaminating star with respect to the local standard determined from images taken under good seeing conditions (0.7 arcsec), from the combined count ratio of V404 Cyg (i.e. V404 Cyg + line-of-sight star) with respect to the local standard. The count ratio of the contaminating star to the local standard is 0.065 and 0.143 in the g' and i' bands respectively. The magnitude of V404 Cyg was then obtained using the observed magnitude of the local standard, $g' = 16.90$ and $i' = 15.12$ (< 0.01 mag uncertainty). The magnitude of the contaminating star was $g' = 19.87$ and $i' = 17.23$. As a check of the photometry and systematics in the reduction and extraction procedures, we also computed lightcurves of a comparison star (13.2" S, 17.1" E of V404 Cyg). The magnitude of the comparison star was $g' = 18.90 \pm 0.03$, $i' = 16.55 \pm 0.02$. The mean g' and i' band magnitudes of V404 Cyg were 19.77 and 16.57 respectively. We estimate the relative photometric accuracy to be 3.0 and 0.9 percent for the 'slow' g' and i' band respectively and 6.0 percent for the 'fast' i' band data.

By co-adding all the images from run 10(b) on Sep 10 taken under good seeing conditions, we estimate $u' = 22.6 \pm 0.7$ for V404 Cyg.

3 BACKGROUND TO V404 Cyg

The X-ray transient GS 2023+338 was discovered during its outburst in May 1989 by the All Sky Monitor aboard the Ginga satellite (Makino 1989). Its high X-ray luminosity suggested that, like other X-ray transients, the system was a close binary with an accreting compact object. The X-ray source was soon identified with the known variable star V404 Cyg, which had been classified as a nova after its 1938 outburst (Marsden 1989).

Spectroscopic observations taken when V404 Cyg was in quiescence revealed the companion to the X-ray source to be a G or early K-type star in an orbit with a period of 6.473 d, which when combined with the secondary star's radial velocity curve implies a mass function of $6.3 \pm 0.3 M_{\odot}$ (Casares, Charles & Naylor 1992). Later on, additional measurements determined the secondary star's rotational broadening, and refined the spectral type of the secondary star and the orbital parameters; the orbital period is $P_{\text{orb}} = 6.4714$ d and semi-amplitude of the secondary star's radial velocity curve is $K_2 = 208.5 \text{ km s}^{-1}$, giving a mass function of $f(M) = 6.08 \pm 0.08 M_{\odot}$ (Casares & Charles 1994). Since this mass function, which provides a firm lower limit to the compact object's mass, exceeds the maximum mass of a neutron star ($\sim 3.3 M_{\odot}$; Cook, Shapiro & Teukolsky 1994), the compact object in V404 Cyg is almost certainly a black hole.

Optical photometry of V404 Cyg in the I -band revealed the secondary star's ellipsoidal variation (Wagner et al. 1992) but these were, however, severely contaminated by short-term variability. Therefore, in an effort to avoid these problems, Shahbaz et al. (1994) observed the lightcurve of V404 Cyg in the K -band, where the flux from the K0IV star is substantially greater (Shahbaz et al. 1996). The analysis of the ellipsoidal variations, which results from the tidal distortion of the secondary star gives the binary inclination angle, combined with spectroscopic observations yields the mass of the binary components. They concluded that the contamination in the infrared was small and deduced the black hole mass to be $12 \pm 2 M_{\odot}$.

Casares et al. (1993) estimated the interstellar reddening to V404 Cyg, by comparing its observed colours with those of a K0III star, after allowing for the accretion disc contribution to the observed flux. They obtained $A_V \sim 4$ and a lower limit of $A_V \sim 3.6$. However, as one can see, the reddening determined in this way depends heavily on the disc contamination in the optical, which the authors measure with large uncertainties. A more accurate determination of the reddening was obtained by Shahbaz et al. (1994) who obtained the K -band lightcurve of V404 Cyg in quiescence and determined the binary inclination angle by modeling the secondary star's ellipsoidal modulation. Assuming that the secondary star is a stripped giant (King 1993) they also determined limits to the reddening and distance to V404 Cyg, by matching the model stripped giant luminosity to that of the secondary star as predicted by the ellipsoidal model. Assuming no disc contamination in the K -band, a reasonable assumption given that the disc contamination measured in the K -band was found to be negligible (Shahbaz et al. 1996), and 10 percent in the V -band, they obtained $2.2 < A_V < 3.3$ (90 percent confidence). Although the determination of the reddening through this method is model dependent, the uncertainties in the disc fraction and

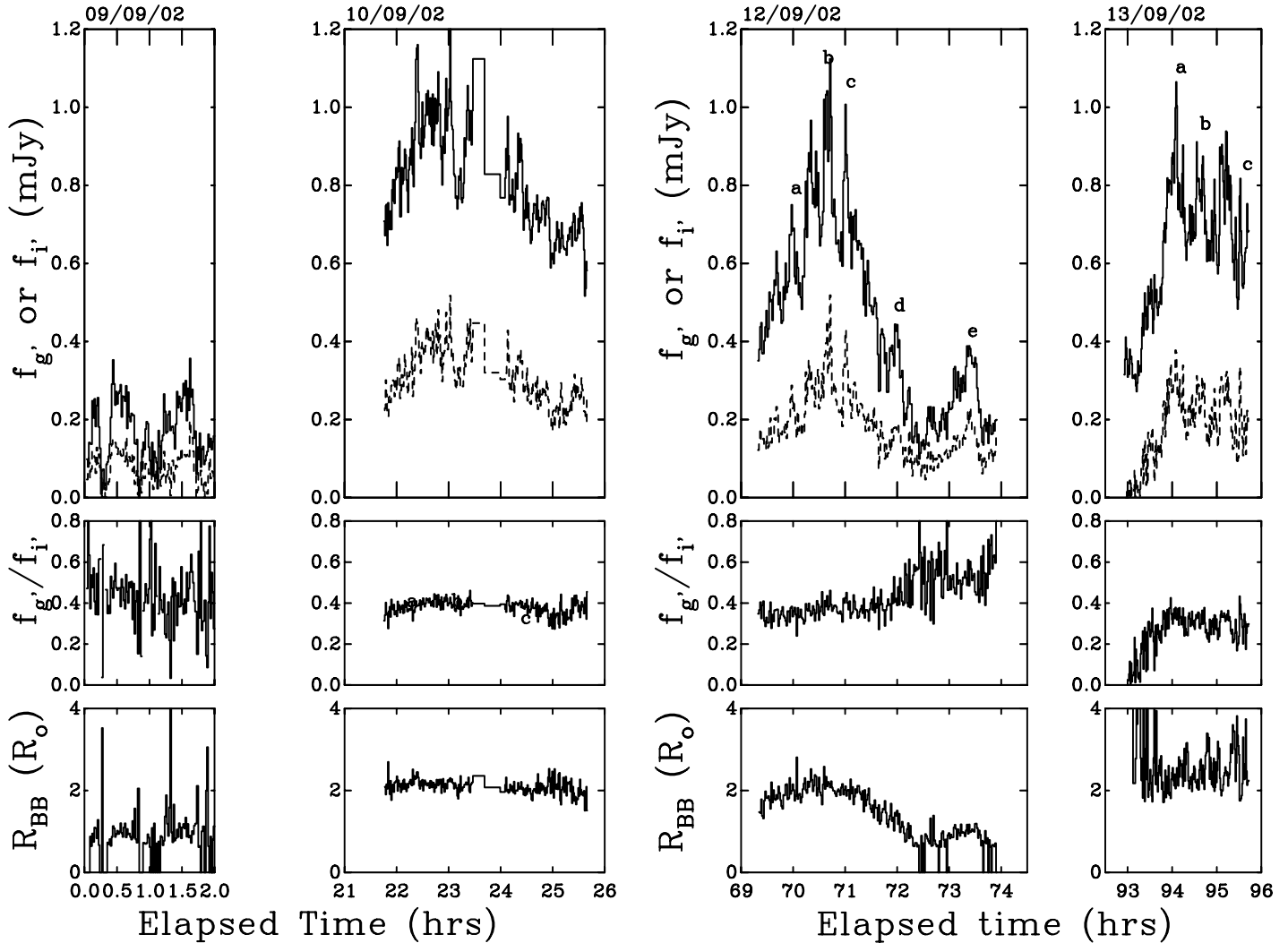


Figure 2. In the top panel we show the flare flux density lightcurve in the g' (dashed line) and i' (solid line) bands, obtained by subtracting the reddened secondary star's ellipsoidal modulation from the observed lightcurves. For clarity the flare lightcurves have been re-binned to a time resolution 1 min. The uncertainties in the g' and i' lightcurves are 0.02 mJy and 0.01 mJy respectively. The letters mark the rapid flare events used to determine the flare properties in Table 2. The middle panels show the flux density ratio $f_{g'}/f_{i'}$ and the bottom panel shows the projected blackbody radius of the region producing the flares.

model dependant parameters such as the binary masses and inclination angle are less in the infrared compared to in the optical. Given the uncertainties in determining the reddening using optical and infrared data, throughout this paper we will use a range of values for the reddening, $2.2 < A_V < 4.0$ and a central value of $A_V = 2.8$.

4 THE LIGHTCURVE OF V404 Cyg

The optical lightcurve of V404 Cyg is dominated by the secondary star's ellipsoidal modulation, which is due to the observer seeing differing aspects of the tidally distorted secondary star. This modulation gives rise to two maxima and minima per orbital cycle. However, superimposed on the ellipsoidal modulation are the large 6 hr flares seen previously (Pavlenko et al. 1996) and also many rapid flares (~ 0.5 hr), similar to what is observed in the short orbital period SXTs (Zurita et al. 2003; Hynes et al. 2003). It is clear that the

secondary star's ellipsoidal modulation is not linked to the variability, therefore if we want to determine the flux of the flares, its contribution must be first removed from the lightcurves.

Figure 1 shows the observed data. Large amplitude flares which last a few hours or more, are observed only on Sep 10, 12 and 13 and are most likely related to the well known 6 hr flare/QPO (Casares et al. 1993; Pavlenko et al. 1996; Hynes et al. 2002). In order to isolate the flux of the flare we assume that the light produced by a flare is simply added to the quiescent spectrum, where the quiescent spectrum is the light from the secondary star's ellipsoidal modulation and the non-variable accretion disc.

We first de-redden the observed magnitudes using the central value for A_V of 2.8 (see section 3) and the ratio $A_V/E(B-V)=3.1$ (Seaton 1979), giving g' and i' extinction values of 3.34 and 1.79 mags respectively and then convert

the Sloan AB magnitudes to flux density. We use the X-ray binary model described in Shahbaz et al. (2003) with the binary mass ratio and inclination angle given in Casares et al. (1993) and Shahbaz et al. (1994) respectively, to determine the ellipsoidal modulation. The model is not set up to compute Sloan magnitudes, so we first compute the Johnson-Cousins magnitudes and then convert to Sloan magnitudes using the colour transformations (Fukugita et al. 1996). We shift the model ellipsoidal lightcurve so as to fit the lower-envelope of the observed lightcurve. We use the data at phase 0.85 (Sep 9) to anchor the fit, since on this night the large 6 hr flare is not seen and so the lower-envelope of these data most likely represents the light from the secondary star and non-variable accretion disc. Figure 1 shows the data and the scaled ellipsoidal model. Clearly the model fails to fit the g' and i' data near phase 0.0 (Sep 10). This suggests that the accretion disc light is variable, most likely due to a residual superhump modulation as is observed in other quiescent SXTs (see Leibowitz, Hemar & Orio 1998; Zurita et al. 2002). This will obviously introduce uncertainties in the subtraction procedure, however, we can obtain a good estimate for the flux of the flares, since on Sep 12 and 13 the model fit partially matches the end and beginning of the large flares respectively. Finally, the scaled ellipsoidal modulation is subtracted from the de-reddened lightcurve yielding the colour of the flares (see Figure 2).

One should note that the conversion from magnitudes to flux density is colour dependant. In order to estimate the scale of this effect, we determine the fluxes obtained using spectra with different power-law indices ($F_\nu \propto \nu^\alpha$). The spectrum of the flares has a mean flux density ratio of $f_{g'}/f_{i'} \sim 0.40$ (see Figure 2) which corresponds to a spectrum with a power-law index of ~ -2 . The ellipsoidal model has a colour ($g' - i'$) = 1.67 which corresponds to a spectrum with a power-law index of -2.8 . Using these models, we estimate that the conversion from Sloan AB mags to flux density units introduces an uncertainty in the colour $f_{g'}/f_{i'}$ of ~ 10 percent. It should also be noted that the residual superhump will introduce an additional uncertainty in the colour of the flare. Since the superhump originates in the outer parts of the disc, it is most likely to have a cool spectrum. Theoretical models for the behaviour of the quiescent accretion disc in V404 Cyg indicates that the outer disc is optically thick and has a temperature of ~ 2000 K (Narayan, Barret & McClintock 1997). If this also represents the colour of the superhump, then assuming the superhump radiates as a blackbody, we estimate that it would add an additional uncertainty of 2 percent in the determination of $f_{g'}/f_{i'}$. Note that these uncertainties are much less than that due to the reddening (see section 4.1).

4.1 The characteristics of the flares

Although large amplitude flares are observed on more than one night, it is only on Sep 10 that a large flare is observed throughout the event. The shape of the large flares seem to be symmetric with similar rise and decay times. Superimposed on these large flares are many rapid events which last typically ~ 0.5 hr. Furthermore, superimposed on these flares, are still shorter term events on timescales of mins which show unresolved peaks (see Figure 3). This makes it difficult to determine the exact shape of the flare events;

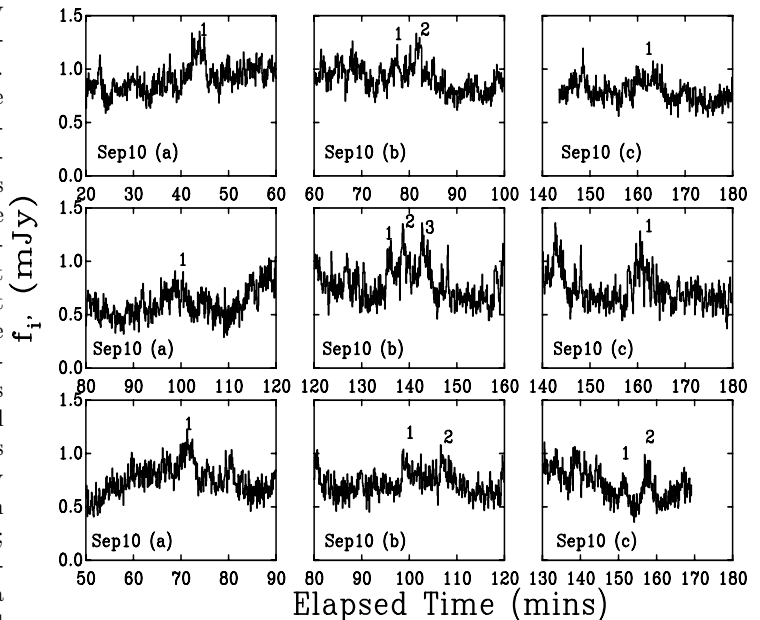


Figure 3. Detailed plots of some individual distinct flares in the i' -band lightcurve. The labelling refers to the events in Figure 2 and Table 2.

there is an indication that some of the flares on the shortest timescales have a burst-like profile [e.g. see flare (b) on Sep 13]. However, in general all the flare events appear to have a linear rise and decay. In Table 2 we estimate some of the characteristics of the individual distinct flares which are shown in Figure 3. The flares typically have a rise time of 2 mins and a duration of 6 mins.

At first sight, one clearly notices that the monochromatic flux in i' is larger than that in g' , at the peak of the large flares, i.e. the flare at its peak has a relatively red spectrum. In general the colour flux ratio $f_{g'}/f_{i'}$ of these flares increases, becoming more blue at the peak. After the peak is reached, the flux and colour decreases becoming more red. The exception is the large flare on Sep 13; the colour seems to increase continuously as the flare proceeds. The most prominent and distinct rapid flares are marked in Figure 2. The mean flux ratio $f_{g'}/f_{i'}$ of the large flares is ~ 0.4 . If we use the extreme values for the reddening $A_V=4.0$ and $A_V=2.2$, then the flux ratio $f_{g'}/f_{i'}$ changes by a factor of 0.53 and 1.36 respectively.

To test if the flaring in the g' and i' bands are simultaneous we calculated the cross-correlation function. The cross-correlation function was symmetric and no time lag was found, so we conclude that the flaring in the two bands is simultaneous (see Figure 4).

5 THE POWER DENSITY SPECTRUM

To compute the PDS of the “slow” data, we use the same flare lightcurves as described in section 4, but since we are only interested in sub-orbital variability, and in order to preserve the flux in each band, we detrend the data for each night using the nightly mean and add on the mean flux level of all the data. Although the sampling of ULTRACAM is

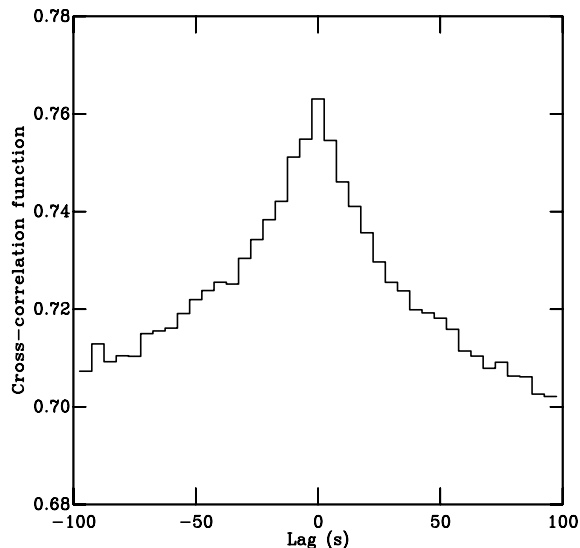


Figure 4. Cross-correlation function between the g' and i' -band lightcurves. A positive lag would indicate that the g' variations lag behind those in i' .

Table 2. Properties of the V404 Cyg flare events. The rise and decay times are obtained from linear fits to the i' band flare profile.

Date	Flare No.	Rise (s)	Decay (s)	PDS power-law index*	
				g'	i'
Sep 10	a ¹	240	110	-1.23	-1.56
	b ¹	104	100		
	b ²	57	58		
	c ¹	65	55		
Sep 12	a ¹	322	242	-0.96	-1.32
	b ¹	62	54		
	b ²	88	44		
	b ³	62	187		
	c ¹	175	241		
Sep 13	a ¹	170	136	-1.17	-1.49
	b ¹	20	96		
	b ²	22	78		
	c ¹	90	130		
	c ²	140	140		

*Power-law index $1-\sigma$ errors of 0.03.

perfectly uniform, we use the method of Lomb-Scargle to compute the periodograms (Press et al. 1992). The Lomb-Scargle method was chosen so that we could combine consecutive runs and confidently compute the periodogram. Also, in order to allow a direct comparison with X-ray PDS, we use the same normalisation method as is commonly used in X-ray astronomy, where the power is normalised to the fractional root mean amplitude squared per hertz. The advantage of this kind of normalisation is that fractional rms amplitudes can be directly estimated from the level of the PDS (van der Klis 1995).

To compute the PDS we use the constraints imposed by the Nyquist frequency and the typical duration of each observation. We then average the PDS for each observing

sequence. We bin and fit the PDS in logarithmic space (Papadakis & Lawrence 1993) and the errors in each bin are determined from the standard deviation of the points within each bin. The white noise level was subtracted by fitting the highest frequencies with a white noise plus red noise model.

5.1 The PDS of the “slow” data

To determine the PDS for the “slow” data we only use the data with the longest baseline i.e. during the nights of Sep 10 and 12. This allows us to extend the PDS to the lowest possible frequencies. The derived PDS is shown in Figure 5. The shape of the g' and i' band PDS are well described by a power-law with slopes of -1.24 ± 0.02 and -1.37 ± 0.02 respectively ($1-\sigma$ errors). On each individual night, the slope of the power-law changes (see Table 2). To examine the systematic effects in our analysis, we also computed the PDS of the comparison star. The PDS was found to be flat, exactly as expected for white noise data. Furthermore, the auto-correlation function of the comparison star is a delta function, implying that the data are not correlated. A QPO feature with a centroid frequency at 0.78 mHz (= 21.5 mins) is present, not surprising given that one can clearly see variability on timescales of 0.5-1.0 hrs in the lightcurves. The fractional root mean squared amplitude is 3 and 1.3 percent for the g' and i' band QPOs and was computed by integrating the Gaussian function and taking the square root.

5.2 The PDS of the “fast” data

We used run14(a), run14(d) and run14(e) to compute the PDS. The other runs were not included because of the high noise level of the data, the result of an increase in the electronic bias level (see section 2). The computed “fast” PDS is shown in Figure 5. The general shape of the PDS has a power-law shape with a slope of -1.16 ± 0.04 ($1-\sigma$ errors). As a check we also computed the PDS of the comparison star. Again the derived PDS was flat, which is exactly as expected for white noise data (see Figure 5).

6 DISCUSSION

6.1 The slope of the PDS

The outer regions of the accretion discs in quiescent SXTs and dwarf novae (DNe) are assumed to be very similar. Therefore if the optical variability observed in the quiescent SXTs originates from these outer regions, then they should have similar properties to those observed in quiescent DNe. Bruch (1992) has performed a study of the rapid variability in cataclysmic variables. The slope of the PDS in quiescent DNe (-1.6 to -2.6) seems to be in general steeper than those observed in quiescent SXTs [-1.0 to -1.52 ; Zurita et al. (2003) and Hynes et al. (2003)]. This suggests that there is either more low-frequency variability in the lightcurves of quiescent DNe compared to quiescent SXTs, or that there is more high-frequency variability in the SXTs. Note that the former could be attributed to intrinsic variability associated with the stream/disc impact region or the white dwarf (e.g. Warner 1995).

On average the slope of the i' PDS in V404 Cyg is

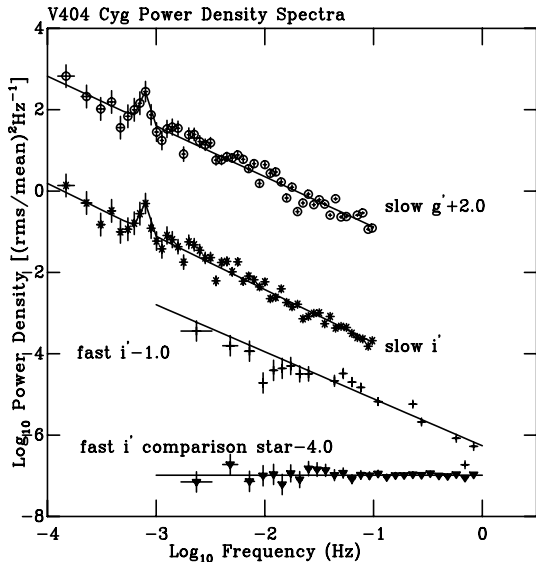


Figure 5. The power density spectrum of V404 Cyg. From top to bottom: V404 Cyg g' and i' “slow” PDS, V404 Cyg i' “fast” PDS and the comparison star PDS.

steeper than the g' slope, suggesting that there is more low-frequency disc variability in i' compared to g' . This difference could be attributed to more variability from outer regions of the disc, such as the stream/disc impact region or more high frequency variability in g' from the inner disk. Thus one expects the slope of the PDS to be dependent on the observed waveband.

Hynes et al. (2003) determined the PDS of the quiescent SXT A0620–00 and found a possible break in the PDS at 0.95 mHz, a feature which is also seen in the low/hard state of SXTs (see Wijnands & van der Klis 1999 and references therein). Although the origin of the break frequency is uncertain, it could be related to the size of the inner advective region; a low break frequency in quiescence would then be expected, as the advective region should be larger. If the break frequency is associated with a dynamical timescale, then it should vary as $R^{1.5}$, where R is the radius of the advective region (see section 6.2). Furthermore, as noted by Hynes et al. (2003) the break frequency most probably scales with some characteristic length scale, which could depend on other parameters, as well as the inner disc radius.

6.2 The QPO feature and the ADAF model

Narayan, McClintock & Yi (1996) and Narayan et al. (1997) showed that the observations of quiescent BH SXTs can be explained by a two-component accretion flow model. The geometry of the flow consists of an inner hot advection-dominated accretion flow (ADAF) that extends from the black hole horizon to a transition radius $r_{\text{tr}} = 10^{4-5} r_{\text{sch}}$ ($r_{\text{sch}} = GM/c^2$ is the Schwarzschild radius for a black hole with mass M) and a thin accretion disk that extends from r_{tr} to an outer radius r_{out} i.e. the radius of the accretion disc. A key feature of the ADAF model of quiescent BH SXTs is its low radiative efficiency. The bulk of the viscously dissipated energy is stored in the gas and is advected with the flow into the black hole. This naturally

explains the unusually low luminosity of BH SXTs, since in NS SXTs, all the advected energy is radiated from the neutron star surface, resulting in a much higher overall radiative efficiency (Narayan & Yi 1995).

An ADAF has turbulent gas at all radii, with a variety of timescales, ranging from a slow timescale at the transition radius down to nearly the free-fall time close to the black hole. In principle, interactions between the hot inner ADAF and the cool, outer thin disk, at or near the transition radius, can be a source of optical variability, due to synchrotron emission by the hot electrons in the ADAF. For an ADAF the variability could be quasi-periodic and would have a characteristic timescale given by a multiple of the Keplerian rotation period at r_{tr} $t_K = 2\pi R/v_K = 2\pi(GM/R^3)^{-1/2} \sim (M/10 M_{\odot})(r/100)^{1.5}$ s, where R is the absolute radius and r is in units of r_{sch} . One also expects slower variations, since the mass supply to the ADAF originates at r_{tr} (Narayan et al. 1997). It should be noted that it is difficult to produce such rapid variations using the thin disc models. Narayan et al. (1997) used the maximum velocity observed in the $H\alpha$ emission line arising from the quiescent thin accretion disc to estimate r_{tr} . However, they note that measuring the maximum velocity is difficult, and so their estimate of $10^{4.4} r_{\text{sch}}$ for r_{tr} should only be considered as an upper limit. If we assume that the 0.78 mHz QPO feature observed in the PDS (see section 5) is the dynamical timescale at the transition radius, then r_{tr} lies at $10^{4.0} r_{\text{sch}}$, which is consistent with that estimated by Narayan et al. (1997). We can write r_{tr} in terms of the accretion disc radius. For the binary parameters of V404 Cyg the outer radius of the disc lies at $r_{\text{out}} = 2.3 \times 10^5 r_{\text{sch}}$ or $12 R_{\odot}$, and so r_{tr} lies at $0.04 R_{\text{disc}}$ or $0.5 R_{\odot}$.

6.3 Comparison of the V404 Cyg QPO features with 4U 1626-67

It is interesting to note the similar timescales of the QPOs we have discovered in V404 Cyg with those found in various X-ray/UV/optical observations of the double-degenerate LMXB, 4U 1626-67. Chakrabarty et al. (2001) used fast CCD photometry to reveal the presence of 3 oscillations: the 130 mHz pulsation (i.e. the well-known 7.66 s X-ray/optical pulsation of the neutron star), a 48 mHz (~ 20 s) QPO (a broad oscillation seen before in X-ray, optical and UV wavebands) and a 1 mHz QPO. This latter oscillation had not been seen before, is not present in any X-ray observations, is quasi-sinusoidal in appearance, and is dramatically stronger in far UV HST data. Chakrabarty et al. (2001) concluded that the first 2 oscillations were clearly X-ray driven and the optical/UV analogues were due to reprocessing in the disc/companion star.

However, the 1 mHz QPO origin is extremely puzzling. The timescale is actually the same as the pronounced X-ray and optical flaring seen from 4U1626-67 during the 1970s and 80s, but this flaring behaviour has vanished since the torque reversal that occurred in 1990. With no X-ray oscillation to drive this process, Chakrabarty et al. (2001) suggested that the 1 mHz QPO is due to “warping” of the inner accretion disc and is of an appropriate timescale for the radius of the inner disc that is set by the magnetospheric corotation radius. In this way, the modulation would be expected to be much greater in the far UV (inner disc) than

the optical (in the outer, shielded regions). It is possible that, in spite of the fact that V404 Cyg almost certainly hosts a $\sim 12 M_{\odot}$ black hole, this analogy can be applied from 4U 1626-67. The difference is in the origin of the truncated inner disc, which for V404 Cyg in X-ray quiescence is expected to be in an ADAF phase (Narayan et al. 1997).

6.4 The emission mechanism of the flares

As one can see from Figure 2, on most of the nights there are numerous rapid flares (< 0.5 hr) superimposed on the single large event (\sim few hrs). Given the uncertainties in the data, it is difficult to determine the shape and hence the physical parameters of these rapid events. We can however comment on the general physical properties of the flares using the large events (\sim few hrs). Using the flare flux density lightcurves we determine the flux density ratio $f_{g'}/f_{i'}$ and the blackbody temperature T_{BB} and equivalent radius R_{BB} . To determine the colour temperature corresponding to a given flux density ratio, we integrate blackbody functions with the CCD and Sloan filter response functions and then determine the $f_{g'}/f_{i'}$ flux density ratio. Given this blackbody temperature we can then determine the corresponding radius of the region that produces the observed dereddened flux at a distance of 3.5 kpc (Casares et al. 1993). Also, using the flux density ratio, the power-law index α of the spectrum ($F_{\nu} \propto \nu^{\alpha}$) can be obtained. One can easily show that the power-law index is given by $\alpha = \Delta \log F_{\nu} / \Delta \log \nu = 4.83 \log(f_{g'}/f_{i'})$.

For Sep 9, the flux density ratio $f_{g'}/f_{i'}$ remains constant at 0.5; α and T_{BB} have constant values of ~ -2 and 5100 K respectively. For the single large flare events on Sep 10 and 13, $f_{g'}/f_{i'}$ is correlated with the flux of the flare; $f_{g'}/f_{i'}$ peaks at ~ 0.3 ; α and T_{BB} peaks at ~ -2.5 and 4100 K respectively. On Sep 12 one can see that the blackbody radius and flare flux are correlated i.e. as the flare flux increases and decreases so does the equivalent blackbody radius. The blackbody radius increases from $\sim 1 R_{\odot}$ to $\sim 2 R_{\odot}$. The same is seen during the decay of the large flare on Sep 10, but to a lesser extent. However, it should be noted that the uncertainties in the reddening (see section 3), which typically correspond to ± 700 K in the T_{BB} estimates, are such that we cannot comment on any colour or temperature variation during the flares.

The peak flux produced by the large flare arises from a region that has a projected blackbody radius of $2 R_{\odot}$ and the rapid flares most likely from smaller regions. In other words, the emitting area at the peak of the large flare covers at least 3 percent of the total disc emitting area. Note that given the data presented here, we cannot state where in the disc these large flares arise. However, it is most likely that the large flares originate in the outer regions of the disc (see section 6.5).

During the large flares observed in V404 Cyg the power-law index of the spectral energy distribution is ~ -2.0 (a range of -1.5 to -2.5 , depending on the flare). It is difficult to explain this in terms of optically thin synchrotron emission, unless the electrons follow a much steeper power-law energy distribution ($N(E)dE \propto E^p dE$). For solar and stellar flares the power-law index of the electron energy distribution p is ~ -2 (Crosby, Aschwanden & Schmitt 1993), which corresponds to a frequency spectrum with a power-law index of $\alpha = -0.5$ ($F_{\nu} \propto \nu^{(1+p)/2}$). The frequency power-law index

observed in V404 Cyg α of ~ -2.0 implies a much steeper index for the electron energy distribution of $p = -5$. However, given the uncertainties in the reddening and therefore in the flux density ratio $f_{g'}/f_{i'}$ (see section 3), we find a range of values for p of -3.6 to -7.5 . It could be that the electrons are thermal and thus do not follow a power-law energy distribution. Also, given that the geometry and physics around a black hole is presumably more extreme, such a steep index for the electron energy distribution is not completely implausible.

The simple model for the flares of blackbody radiation from a heated region of the disc's photosphere (i.e. photospheric in origin) is unlikely. A more likely model for a thermal flare is emission from an optically thin layer of recombining hydrogen, which is essentially the mechanism generally accepted for solar flares. We therefore determine the continuum emission spectrum of an LTE slab of hydrogen and then calculate the expected flux density ratio $f_{g'}/f_{i'}$ in the g' and i' bands using the same method as the blackbody case. We find that a continuum slab temperature of 8000 K with a baryon column density of 10^{22} cm^{-2} (taken from Welsh, Horne & Oke 1993) gives $f_{g'}/f_{i'} = 0.30$; propagating the uncertainty in the reddening (see section 3), we find the range for the slab temperature to be 5500 K and 9100 K. It should be noted that the hydrogen slab model does not include the contribution from Balmer emission lines. Since the g' filter includes $H\beta$, our determination of the flux density ratio $f_{g'}/f_{i'}$ is biased. However, we can estimate the amount of bias given the $H\beta$ flux and equivalent width, 0.20 mJy and 10 \AA respectively (Casares et al. 1993). Since the g' filter has a width of $\sim 2000 \text{ \AA}$ the contribution of the $H\beta$ emission line to the g' flux density in V404 Cyg is only 1 percent, in contrast to that in AE Aqr (Welsh, Horne & Oke 1993).

Since we only have observations in two wavebands, we cannot accurately determine the physical parameters of the flares. However, it should be noted that the spectrum of the flare seems to be similar to that observed in AE Aqr (Welsh, Horne & Oke 1993). Using the colour information for the large flare events, we can say that the large flares arise from a region which extends a projected area which has an equivalent R_{BB} of $\sim 2 R_{\odot}$. One should regard the equivalent R_{BB} estimate as a lower limit, because the emission mechanism is unlikely to be blackbody. In general the rapid flares seem to arise from optically thin gas which has a peak temperature of ~ 8000 K in the continuum. However, to obtain a more accurate estimate of the physical conditions of the flares, one must resolve the Balmer jump and Paschen continuum.

Spectroscopic observations suggest that the whole disc participates in the large flares, since the whole $H\alpha$ emission line profile changes (Hynes et al. 2002). This seems to contradict our earlier results, which suggest that the large flares arise from regions that cover only 3 percent of the disc's total area. However, this most likely indicates that the emission is optically thin, or that the emission area is small. Also, given the low resolution of the spectroscopy, we can only really say that material from all around the disc is contributing, given that the line profile changes observed extend across the whole line profile and appear double-peaked. It is not possible to exclude the flares from arising from only the inner regions of the disc.

6.5 Where are the flares produced?

Zurita et al. (2003) have presented arguments that suggest the most likely mechanism for the flares is by local magnetic reconnection events in or above the accretion disc. It is believed that a dynamo mechanism, driven by the strong shear produced by differential rotation, operates in accretion discs (Tout & Pringle 1992). Regions of oppositely directed magnetic fields develop within the disc or between the disc and corona and reconnect explosively, resulting in a flare (Haswell, Tajima & Sakai 1992b). The duration of the flare is directly related to the shearing timescale. As suggested by Zurita et al. (2003), assuming that the range of flare durations observed in the SXTs reflect their location in the accretion disc, then the flares with the longest duration represent the shearing timescale in the outer parts of the disc. Thus the maximum flare duration should be limited by the outer disc radius and V404 Cyg should show short-term variability, similar to what is observed in A0620–00. The very rapid flares (\sim mins) observed in V404 Cyg (see Figure 3) have a similar timescale to those observed in A0620–00 (Hynes et al. 2003) and seems to support the scenario that the large flares (\sim few hrs) are produced in regions further out in the disc than the rapid (\sim 0.5 hr) and very rapid (\sim mins) flares.

Using the colour information about the large events (\sim hrs), we can say that the large flares are produced from a region which extends an equivalent blackbody radius of $\sim 2R_{\odot}$. We cannot determine the emitting area of the rapid flares (\sim 0.5 hr) as the result may be biased due to the large flares. However, if our interpretation of the 21.5 min QPO feature is correct, then these rapid flares are most likely produced near the transition radius of the ADAF, in the inner parts of the disc. We cannot determine the exact mechanism for the flare production. The flares could arise in optically thin gas with a temperature of ~ 8000 K, most likely in a corona above the accretion disc, or from optically thin synchrotron emission.

Nayakshin & Svensson (2001) have argued that an ADAF model is not required to reproduce the observed X-ray luminosities of quiescent SXTs. They propose a model which consists of a standard thin disc with a hot corona, powered by magnetic flares. Although this scenario seems appealing, it is difficult to see how the thin disc model could produce rapid variations. However, it should be noted that the explosive magnetic reconnection model described in Haswell, Tajima & Sakai (1992b) could produce rapid variations from a thin disc, similar to an ADAF. Our observations suggest that for the rapid flares (\sim 0.5 hr) at least, they are produced near the transition radius. However, it is only by obtaining precise velocity information about the flares, can we begin to place constraints on the exact location of the flares in the accretion disc.

ACKNOWLEDGMENTS

TS acknowledges support from the Spanish Ministry of Science and Technology under project AYA200203570. RIH is currently supported by NASA through Hubble Fellowship grant #HF-01150.01-A awarded by the Space Telescope Science Institute, which is operated by the Association of Universities for Research in Astronomy, Inc., for NASA, under

contract NAS 5-26555. VSD and TRM acknowledge the support of PPARC through the grant PPA/G/S/1998/00534. Based on observations made with the William Herschel Telescope operated on the island of La Palma by the Isaac Newton Group in the Spanish Observatorio del Roque de los Muchachos of the Instituto de Astrofísica de Canarias.

REFERENCES

- Bruch A., 1992, *A&A*, 266, 237
 Casares J., Charles P.A., 1992, *MNRAS*, 255, 7
 Casares J., Charles P.A., Naylor T., 1992, *Nat*, 355, 614
 Casares J., Charles P.A., Naylor T., Pavlenko E.P., 1993, *MNRAS*, 265, 834
 Casares J., Charles P.A., 1994, *MNRAS*, 271, L5
 Chakrabarty D., Homer L., Charles P.A., O'Donoghue D., 2001, *ApJ*, 562, 985
 Cook G.B., Shapiro S.L., Teukolsky S., 1994, *ApJ*, 424, 823
 Crosby N.B., Aschwanden M.J., Schmitt J.H.M.M., 1993, *Sol.Phys.*, 143, 275
 Dhillon V., Marsh T.R., 2001, *NewAR*, 45, 91
 Esin A.A., McClintock J.E., Narayan R., 1997, *ApJ*, 489, 865
 Esin A.A., McClintock J. E., Drake J.J., Garcia M.R., Haswell C. A., Hynes R. I., Munro M. P., 2001, *ApJ*, 555, 483
 Fukugita M., Ichikawa T., Gunn J.E., Doi M., Shimasaku K., Schneider D.P., 1996, *AJ*, 111, 1748
 Haswell C.A., Tajima T., Sakai J.-I., 1992, *ApJ*, 401, 495
 Hjellming R.M., Rupen M.P., Mioduszewski A.J., Narayan R., 2002, *ATel*, 54
 Hynes R.I., Zurita C., Haswell C.A., Casares J., Charles P.A., Pavlenko E.P., Shugarov S.Yu., Lott D.A., 2002, *MNRAS*, 330, 1009
 Hynes R.I., Charles P.A., Casares J., Haswell C.A., Zurita C., Shahbaz T., 2003, *MNRAS*, 340, 447
 King A.R., 1993, *MNRAS*, 260, L5
 Kong A.K.H., McClintock J.E., Garcia M.R., Murray S.S., Barret D., 2002, *ApJ*, 570, 277
 Leiowitz E.M., Hemar S., Orío M., 1998, *MNRAS*, 300, 463
 Marsden B.G., 1989, *IAU Circ* 4783
 Markino F. et al., 1989, *IAU Circ* 4782
 Narayan R., Garcia M. R., McClintock J. E., 2001, in *proc. IX Marcel Grossmann Meeting*, eds. V. Gurzadyan, R. Jantzen, R. Ruffini, World Scientific (Singapore), astro-ph/0107387
 Narayan R., Barret D., McClintock J.E., 1997, *ApJ*, 482, 448
 Narayan R., McClintock J.E., Yi I., 1996, *ApJ*, 457, 821
 Narayan R., Yi I., 1995, *ApJ*, 452, 710
 Nayakshin S., Svensson R., 2001, *ApJ*, 55, L67
 Papadakis I.E., Lawrence A., 1993, *MNRAS*, 261, 612
 Pavlenko E.P., Martin A.C., Casares J., Charles P.A., Ketsaris N.A., 1996, *MNRAS*, 281, 1094
 Press W.H., Teukolsky S.A., Vetterling W.T., Flannery B.P., 1992, *Numerical Recipes*, 2nd Edn., CUP, Cambridge
 Sanwal D., Robinson E.L., Zhang E., Colome C., Harvey P.M., Ramseyer T.F., Hellier C., Wood J.H., 1996, *ApJ*, 460, 437
 Seaton M.J., 1979, *MNRAS*, 187, 73

- Shahbaz T., Ringwald F.A., Bunn J.C., Naylor T., Charles P.A., Casares J., 1994, MNRAS, 271, L10
- Shahbaz T., Bandyopadhyay R., Charles P.A., Naylor T. 1996, MNRAS, 282, 977
- Shahbaz T., Zurita C., Casares J., Dubus G., Charles P.A., Wagner R.M., Ryan E., 2003, ApJ, 585, 443
- Smith J.A., et al., 2002, AJ, 123, 2121
- Tout C.A., Pringle J.E. 1992, MNRAS, 259, 604
- van der Klis M., 1995, in X-ray Binaries, eds. W. H. G. Lewin, J. van Paradijs, E. P. J. van den Heuvel, CUP, p. 252
- van Paradijs J., McClintock J.E., 1995, in X-ray Binaries, eds. W. H. G. Lewin, J. van Paradijs, E. P. J. van den Heuvel, CUP, p. 58
- Wagner R.M. Kreidl T.J., Howell S.B., Starrfield S.G., 1992, ApJ, 401, L97
- Wagner R.M., Starrfield S.G., Hjellming R.M., Howell S.B., Kreidl T.J., 1994, ApJ, 429, L25
- Warner, B. 1995, Cataclysmic Variables, Cambridge Astrophysics Series, Cambridge University Press
- Welsh W.F., Horne K., Oke J.B., 1993, ApJ, 406, 229
- Wijnands R., van der Klis M., 1999, ApJ, 514, 939
- Zurita C., Casares J., Shahbaz T., 2003, ApJ, 582, 369
- Zurita C. et al., 2002, MNRAS, 333, 791